Preparation of a Ni/$LaAlO_3$ Catalyst and its Application in Catalytic Pyrolysis of Soybean Straw for Syngas Production

Zeshan Li, Weitao He, Tao Xiong, Yan Wang, Juanjuan Zhang, Chaoqiang Guo, Kui Lan, Shuang Shang, Yiran Zhang, and Jianfen Li*

A $LaAlO_3$ carrier was prepared *via* the sol-gel method, and a Ni/$LaAlO_3$ catalyst was prepared *via* the homogeneous precipitation method; this catalyst was used for the catalytic pyrolysis of soybean straw for syngas (H_2 + CO) production. The analysis of the raw materials (straw) was performed *via* elemental analysis and industrial analysis. The support and catalyst were characterized and analyzed by X-ray fluorescence spectroscopy, thermogravimetric analysis, X-ray diffraction, scanning electron microscopy, and N_2 adsorption-desorption isotherms. The results illustrated that the NiO was uniformly loaded on the $LaAlO_3$ surface. Furthermore, the effects of the Ni loading amount, pyrolysis temperature, holding time, and calcination temperature on the performance of the catalyst were studied. The results showed that the catalyst had the highest increase in production and concentration of H_2 and CO when the Ni loading was 10 wt%, the calcination temperature was 500 °C, the reaction temperature was 800 °C, and the holding time was 20 min. Compared with the pyrolysis of straw without a catalyst, the yield of H_2 and CO increased from 85 mL/g and 125 mL/g to 238.5 mL/g and 255 mL/g, respectively, and the concentration of H_2 and CO increased from 23.5 vol% and 29.4 vol% to 43.1 vol% and 41.9 vol%, respectively.

Keywords: $LaAlO_3$; Catalytic pyrolysis; Soybean straw; Syngas

*Contact information: School of Chemical and Environmental Engineering, Wuhan Polytechnic University, Wuhan 430023 China; *Corresponding author: lijfen@163.com*

INTRODUCTION

With the continued development of society and the economy, energy and environmental issues have become increasingly prominent, especially the increase in energy consumption, which is led by fossil energy. The development and consumption of fossil energy will eventually become unsustainable (Saxena *et al.* 2009). Biomass is a renewable raw material that can be produced with straw (among other materials), which can be converted into solid, liquid, and gas fuels through chemical and biological processes (Zhao and Yan 2012). Pyrolysis is one of the most effective technologies for converting biomass into fuel. The products are gas, tar, and coke. However, the yield of syngas produced *via* the pyrolysis of straw in the absence of a catalyst is low, the combustible gas content is low, the calorific value is low, and a large amount of tar is generated. The tar in the gas is easily condensed at low temperatures, and it has a long accumulation time, which leads to pipe blockages and other problems (Hossain *et al.* 2016). Moreover, it will cause energy loss and environmental problems related to tar.

However, the formation of toxic and harmful organic compounds can be avoided. Increased attention has been paid to catalytic reforming technology, which can convert

biomass, *i.e.*, straw, into syngas with almost no tar at a lower temperature (Li *et al.* 2013). Nickel-based catalysts are widely used for gasification, tar conversion, and the reformation of light hydrocarbons due to their high tar destructive activity and ability to increase the content of syngas in the produced gas (Li *et al.* 2009; Li *et al.* 2014; Gao *et al.* 2017).

Commonly used nickel-based catalyst supports are divided into metal oxides (Al_2O_3, MgO, *etc.*), natural ores (dolomite, olivine, and palygorskite), and natural zeolite molecular sieves (Xu *et al.* 2013; Zou *et al.* 2017; Lian *et al.* 2018; Tan *et al.* 2019; Li *et al.* 2020). Li *et al.* (2013) prepared a NiO/γ-Al_2O_3 catalyst for the steam reforming of rice biomass, and they compared the performance of SiO_2, CaO, and TiO_2 as a support catalyst. The results showed that γ-Al_2O_3 had better performance, better tar catalytic cracking ability, and drastically improved hydrogen production. However, a catalyst based on an alumina support did not yield positive results in terms of coke deposition, due to its strong acidity. Wei *et al.* (2018) synthesized mesoporous Ni-Mg-Al and Ni-Al catalysts and used them in the dry reformation of methane and the coupling reformation of a partial oxidation reaction of methane. The results showed that compared to Ni-Al and Ni/Al_2O_3 catalysts, Ni-Mg-Al catalysts had a larger surface area, higher Ni dispersion, smaller Ni particle size, higher gas (H_2 + CO) synthesis, and excellent stability. Loy *et al.* (2018) found that compared with the commercial catalysts (nickel and natural zeolite) in rice husk catalytic pyrolysis, using coal bottom ash catalyst can generate higher syngas content and lower coke formation. Chein and Fung (2019) studied the application of CeO_2 modified Ni/Al_2O_3 catalyst in dry reforming of methane to syngas. It was found that CeO_2 promoted the reaction of DMR. When O_2 was added to the reaction, the carbon deposition of CeO_2 modified Ni/Al_2O_3 catalyst was the lowest. Claude *et al.* (2019) studied the properties of Ni/γ-Al_2O_3 catalyst prepared by the sol-gel method and the wet impregnation method. It was found that the catalyst prepared by the sol-gel method had more stable catalytic activity and lower carbon deposition. Zhao *et al.* (2019) used NiAl-LDHs/FeCrAl fiber as the catalyst precursor and prepared Ni-$CeAlO_3$-Al_2O_3/FeCrAl fiber flakes for COMR process by thermal delamination, CeO_2-modification, and H_2-reduction. The use of a "$CeAlO_3$-CeO_2" cycle enables the catalyst with high carbon resistance because of the intensified C-elimination to inhibit filaments growth. Perovskite composite oxides have unique crystal structures, especially the crystal defect structure and the properties formed after doping, which has multiple applications as a replacement to precious metals, such as its usage as or in solid fuel cells, solid electrolytes, sensors, high temperature heating materials, solid resistors, and oxidation-reduction catalysts. As such, this material has become a research hotspot in the fields of chemistry, physics, and materials. Figueredo *et al.* (2018) studied and compared the use of perovskite $LaAlO_3$ and commercial α-Al_2O_3 supported nickel catalyst in the dry reformation of methane. It was found that perovskite type $LaAlO_3$ had a more stable performance than Al_2O_3, and the $LaAlO_3$ was prepared *via* a microwave assisted thermal method. However, the preparation of $LaAlO_3$ as a catalyst carrier by sol-gel method has rarely been reported. La as a metal carrier can improve the activity of nickel catalyst and prevent sintering. The amount of La is small and the cost increases slightly. Therefore, the $LaAlO_3$ carrier was prepared by sol-gel method, and then Ni/$LaAlO_3$ accelerator was prepared by homogeneous precipitation method. The raw materials were characterized by elemental analysis, XRF, XRD, SEM, and BET. The pyrolysis experiments of soybean straw were carried out. The effects of nickel loading, reaction temperature, holding time and calcination temperature of the catalyst on the performance and stability of the catalyst were investigated.

EXPERIMENTAL

Materials

Soybean straw (SS), which was collected in Lvliang, Shanxi province, China, was chosen as the biomass feed stock in this study. Prior to testing, the soybean straw was crushed and sieved to obtain particles that were size 60 mesh and lower. The straw was then dried at 105 °C for 24 h, and then sealed in the drying oven to eliminate the introduction of additional moisture content. The ultimate and proximate analysis of the soybean straw samples (as shown in Table 1) were both conducted using an elemental analyzer (Flash 2000, Thermo Fisher Scientific, Waltham, MA) and according to GB/T standard 28731 (2012).

Table 1. Proximate and Ultimate Analyses of the Soybean Straw

Materials	Ultimate Analysis (wt%)					Proximate Analysis (wt%)			
	C	H	O*	N	S	M	A	V	FC
Soybean Straw	40.08	5.53	53.33	1.06	0	9.1	8.6	77.76	4.54
* by difference; M: Moisture; V: Volatile matter; A: Ash; FC: Fixed Carbon									

Preparation of support and catalyst

All reagents used were purchased from Aladdin industries (Shanghai, China).

$LaAlO_3$ was prepared *via* the sol-gel method. 4.6g $La(NO_3)_3 \cdot 6H_2O$ and 9.6g citric acid were mixed and dissolved in deionized water, and 5.4g $Al(NO_3)_3 \cdot 9H_2O$ was dissolved in deionized water and stirred, making it completely dissolved. Then it was poured into a lanthanum nitrate citric acid mixture, stirred vigorously for 1 h, then evaporated into a gel. The material was put it in a 200 ℃ oven to dry overnight, and then it was placed in a 800 ℃ muffle furnace for calcination.

$Ni/LaAlO_3$ catalyst was prepared *via* the homogeneous precipitation method with $Ni(NO_3)_2 \cdot 6H_2O$ as the nickel precursor and $LaAlO_3$ as the support. First, 5 g of $LaAlO_3$ was placed in a 500 mL three neck flask, and then $Ni(NO_3)_2 \cdot 6H_2O$ and CON_2H_4 (in a mass ratio of 1:4) were mixed with 100 mL of deionized water.

After the mixture was completely dissolved, it was poured into a three-neck flask, stirred in an oil bath at 115 °C for 2 h, and aged for 2 h. Next, the mixture was filtered and washed. It was then dried at 105 °C for 12 h. The dried catalyst precursor was calcined in a muffle furnace at a set temperature for 2 h to obtain the catalyst ($NiO/LaAlO_3$). The catalysts were prepared with different parameters, as follows: a Ni loading amount of 5 wt%, 10 wt%, 15 wt%, or 20 wt% and a calcination temperature of 500 °C, 600 °C, 700 °C, or 800 °C.

Instruments and Experimental Methods

The experimental device is shown in Fig. 1, which included a gas supply system, pyrolysis reactor, gas purification device, gas collection bag, and analysis system. The tests were conducted in a horizontal fixed-bed quartz tube reactor. The furnace was on the top of the tube reactor and surrounded the quartz tube to ensure that it was heated. Two quartz boats were each used to separately hold the biomass and catalyst, with an inner diameter of 40 mm, a length of 100 mm, and a height of 10 mm.

The gas purification device was placed in an ice water bath to completely eliminate the influence of tar. The reactor had an inner diameter of approximately 60 mm, had a total length of 1400 mm, and had a flat-temperature zone of 600 mm.

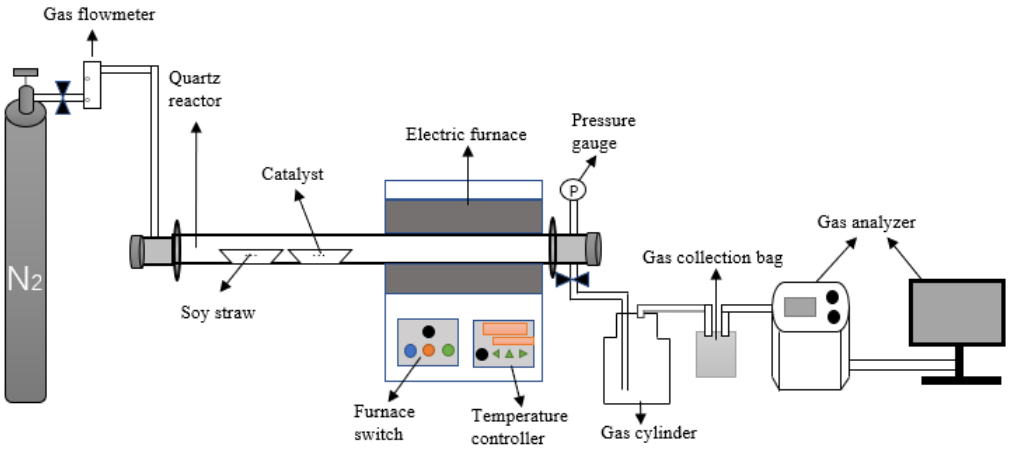

Fig. 1. Schematic diagram of the experimental system

First, 2 g of straw and 0.5 g of catalyst were put into two quartz boats in the reactor, and then the flanges on both sides were closed. Nitrogen at a flow rate of 100 mL/min was continuously introduced into the entire system for 30 min under room temperature to ensure an oxygen-free environment. Subsequently, the reactor temperature was increased from room temperature to the specified temperature (600 °C, 700 °C, 800 °C, or 900 °C,) at a heating rate of 10 °C/min and maintained for a specified time (5 min to 30 min). When the flat-temperature zone was preheated to the target temperature, the two boats were quickly pushed to the furnace. After the reaction time reached the set time, the furnace was pushed away and the valves on both sides of the tube were opened. Meanwhile, the syngas was collected in the gas sample bag. Finally, the gas composition and content of the syngas were determined *via* the gas analyzer. Each group of tests was repeated three times to take the average value to ensure the reliability of the collected data.

Methods

The elemental composition and material structure of the catalysts were analyzed *via* X-ray fluorescence spectrometer (EDX-7000, SHIMADZU, Kyoto, Japan) and X-ray diffraction (XRD-7000, SHIMADZU, Kyoto, Japan). A thermogravimetric analyzer (SDT Q600, TA Instruments, New Castle, DE) was used to evaluate the thermal stability of the support, catalyst, and used catalyst. The specific surface area and pore structure of the support, catalyst, and used catalyst were measured *via* a surface area analyzer (ASAP 2020 HD88, Micromeritics, Norcross, GA). The microstructure of the support, catalyst, and used catalyst were analyzed *via* scanning electron microscopy (S-3000N SEM, HITACHI, Tokyo, Japan). The volatile gas was collected with a gas sample bag and analyzed *via* an infrared gas analyzer (Gasboard-3100, Cubic-Ruiyi, Wuhan, China). Considering that the relative content of CH_4 and other hydrocarbons (C_nH_m) could be neglected, this experiment only evaluated the performance of the catalysts by measuring the synthesis gas content (H_2 + CO).

RESULTS AND DISCUSSION

Characterization of the Ni/$LaAlO_3$ Catalyst

X-ray fluorescence analysis

The elemental compositions of the $LaAlO_3$ and Ni/$LaAlO_3$ catalysts are shown in Table 2. The XRF analysis showed that the main components of the support were La and Al. The support was calcined in air to form $LaAlO_3$. After the nickel was loaded, it oxidized into NiO after being calcined by a muffle furnace. The loading amount of NiO in the catalyst was consistent with the theoretical loading amount.

Table 2. XRF Analyses of the $LaAlO_3$ and Ni/$LaAlO_3$ Catalyst

Sample	Main Composition and Content (wt%)		
	La_2O_3	Al_2O_3	NiO
$LaAlO_3$	77.78	19.22	0
Ni/$LaAlO_3$	70.75	16.87	11.29

X-ray diffraction analysis

Figure 2 shows the XRD spectra of the $LaAlO_3$ and Ni/$LaAlO_3$ catalysts. There were some characteristic peaks at 2θ at values of 23.3°, 33.5°, 41.2°, 47.9°, 54.0°, 59.6°, 70.1°, 75.0°, 79.9°, and 84.6°, which could be identified as the characteristic peaks of $LaAlO_3$ (PDF # 70-4108). The peaks at 27.7°, 43.3°, and 63.9° were identified as characteristic NiO peaks (PDF # 78-0429), which indicated that NiO/$LaAlO_3$ was formed after the catalyst was calcined. Therefore, it was concluded that the Ni existed in the form of NiO, which coincided with the XRF analysis. The peaks at 44.4° and 51.7° were identified as the characteristic peaks of Ni (PDF # 89-7128), and the active component changed from NiO to elemental Ni.

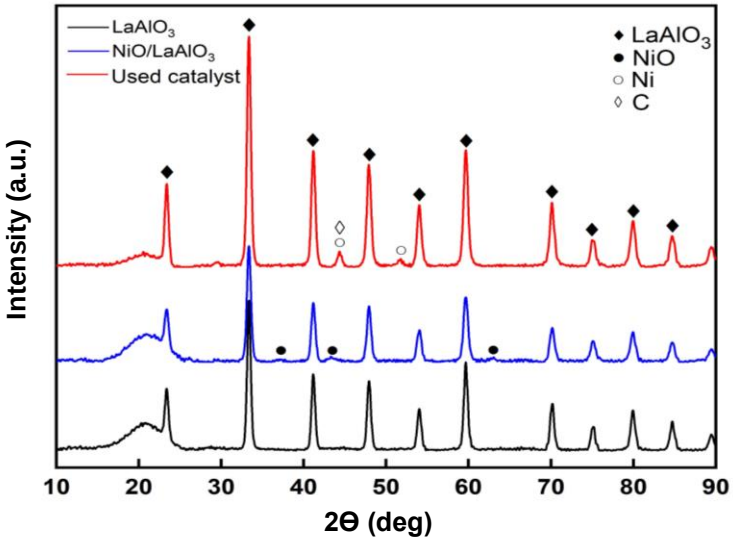

Fig. 2. The XRD patterns of $LaAlO_3$ and Ni/$LaAlO_3$ catalysts

Hu *et al.* (2018) showed that the conversion of NiO to Ni through hydrogenation reduction could help improve tar conversion rates. The peak at 44.3° was identified as the characteristic peak of C (PDF # 80-0017), which indicated a small amount of carbon

deposits on the catalyst surface. Due to the formation of these carbon deposits, the catalyst pore structure would become blocked, such that the active sites of the catalyst were covered. Therefore, the catalyst activity would decrease after being used.

Thermogravimetric analyzer

The thermogravimetric curves of $LaAlO_3$ and $Ni/LaAlO_3$ are shown in Fig. 3. As shown, the TG curves of the carrier and the catalyst were almost straight lines, which indicated that the carrier and the catalyst had good thermal stability. This high thermal stability provided good support for subsequent experiments.

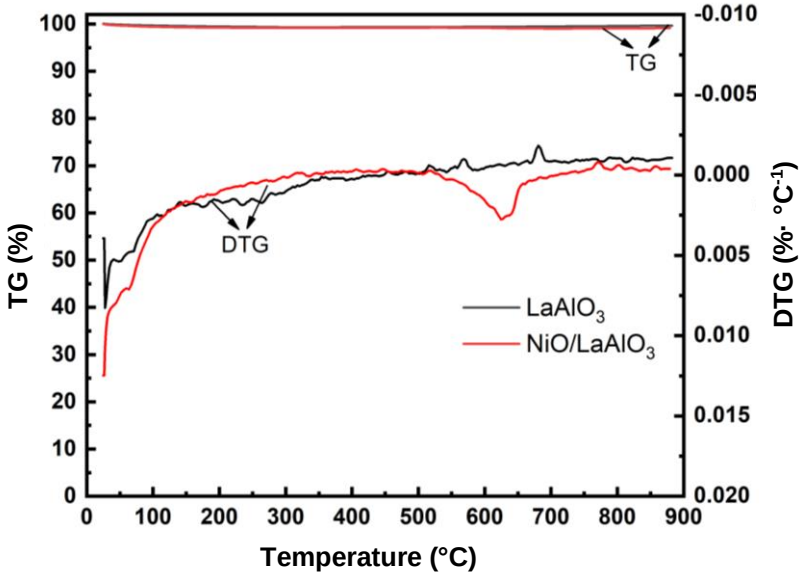

Fig. 3. Thermogravimetric analyzer of $LaAlO_3$ and $Ni/LaAlO_3$

Temperature program reduction (TPR)

According to the TPR-H_2 curve (Fig. 4), the reduction temperature of Ni/ $LaAlO_3$ catalyst is between 249 and 478 °C, but there are two shoulders between 95 and 241 °C.

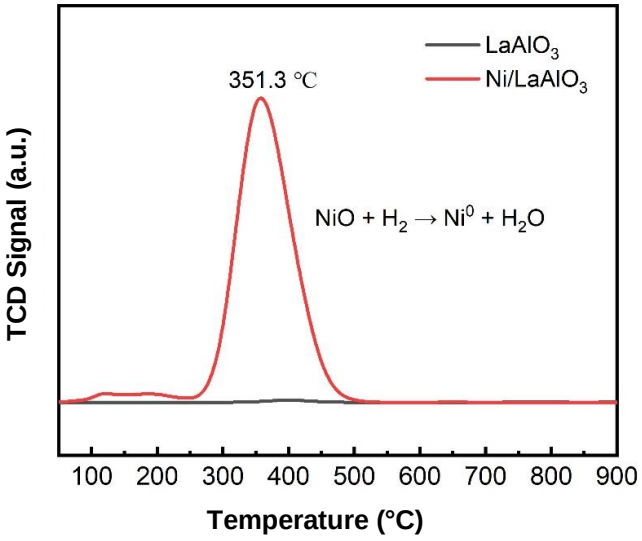

Fig. 4. TPR analysis results for $LaAlO_3$ and $Ni/LaAlO_3$

This may be attributed to the easy removal of O^{2-} ions from NiO/$LaAlO_3$ interface. This is the particularity of Ni/$LaAlO_3$ catalyst, because the pure $LaAlO_3$ carrier does not show the reduction curve (Fig. 4). Although the contribution of these two events to the reduction curve of Ni/$LaAlO_3$ is very small, their role in catalyst activation may be very important due to the vacancy on the NiO/support interface.

Scanning electron microscope analysis

The surface morphology of the $LaAlO_3$ support, Ni/$LaAlO_3$ catalyst, and used Ni/$LaAlO_3$ catalyst are presented in Fig. 5. The support had a mesoporous structure, as shown in Fig. 5a, which could allow for NiO to be uniformly loaded on the surface of the support, as shown in Fig. 5b. This was consistent with the BET analysis results, and it effectively increased the active surface area and provided more contact parts for tar cracking in the gas. Figure 5c showed that the used Ni/$LaAlO_3$ catalyst particles had agglomerated, the particle size was not uniform, and it was covered with carbon, which resulted in decreased catalyst activity (Xiao *et al*. 2013).

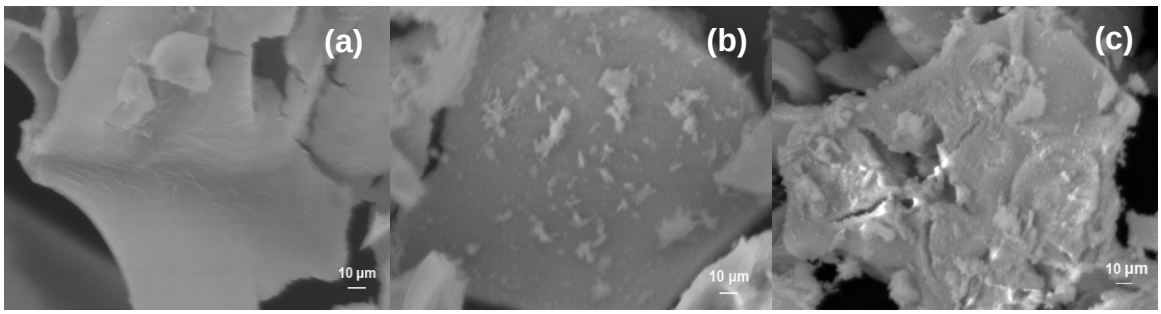

Fig. 5. SEM images of (a) $LaAlO_3$, (b) Ni/$LaAlO_3$, and (c) used Ni/$LaAlO_3$

Analysis of specific surface area and pore structure

The $LaAlO_3$, Ni/$LaAlO_3$, and used Ni/$LaAlO_3$ N_2 adsorption-desorption isotherms, as well as the BJH pore size distributions, are shown in Fig. 6, and the related parameters are shown in Table 3. The N_2 adsorption-desorption isotherms of the three samples had obvious hysteresis loops. According to IUPAC classification, all the isotherms conformed to the IV model. The pore sizes of the $LaAlO_3$ support and Ni/$LaAlO_3$ catalyst were mainly distributed between a range of 50 nm to 250 nm, and the pore sizes of the used Ni/$LaAlO_3$ catalyst were mainly distributed within a range of 50 nm to 175 nm. This further indicated that the three samples had a mesoporous structure. The mesoporous structure of the catalyst was conducive to the further adsorption of tar, which promoted full contact between the tar and the active components, which led to additional cracking, *i.e.*, an increase in syngas production. According to Table 3, the BET surface areas of the $LaAlO_3$ support, the Ni/$LaAlO_3$ catalyst, and the used Ni/$LaAlO_3$ catalyst were 12.63, 22.11, and 14.52 $m^2 \cdot g^{-1}$, respectively. In addition, it was shown that the specific surface area and pore volume of the Ni-supported catalyst was increased when compared to the $LaAlO_3$ support. However, the pore diameter decreased, which suggested that the addition of Ni to the $LaAlO_3$ structure increased the level of Ni dispersion (Lim *et al.* 2007). The Ni in the perovskite catalyst could become more reducible than the $LaAlO_3$, which would lead to the formation of small particle on the surface and more abundant dispersion (Lim *et al.* 2009). The decrease in specific surface area and pore volume of the used Ni/$LaAlO_3$ was due to a small amount of carbon deposits on the catalyst surface after the reaction, which was consistent with the SEM analysis results.

Table 3. Textural Parameters of $LaAlO_3$, $Ni/LaAlO_3$, and Used $Ni/LaAlO_3$

Sample	$LaAlO_3$	$Ni/LaAlO_3$	Used $Ni/LaAlO_3$
BET Surface Area ($m^2 \cdot g^{-1}$)	12.6309	22.1070	14.5179
Total Pore Volume ($cm^3 \cdot g^{-1}$)	0.097950	0.165453	0.115160
Average Pore Diameter (d/nm)	110.434	109.872	121.142

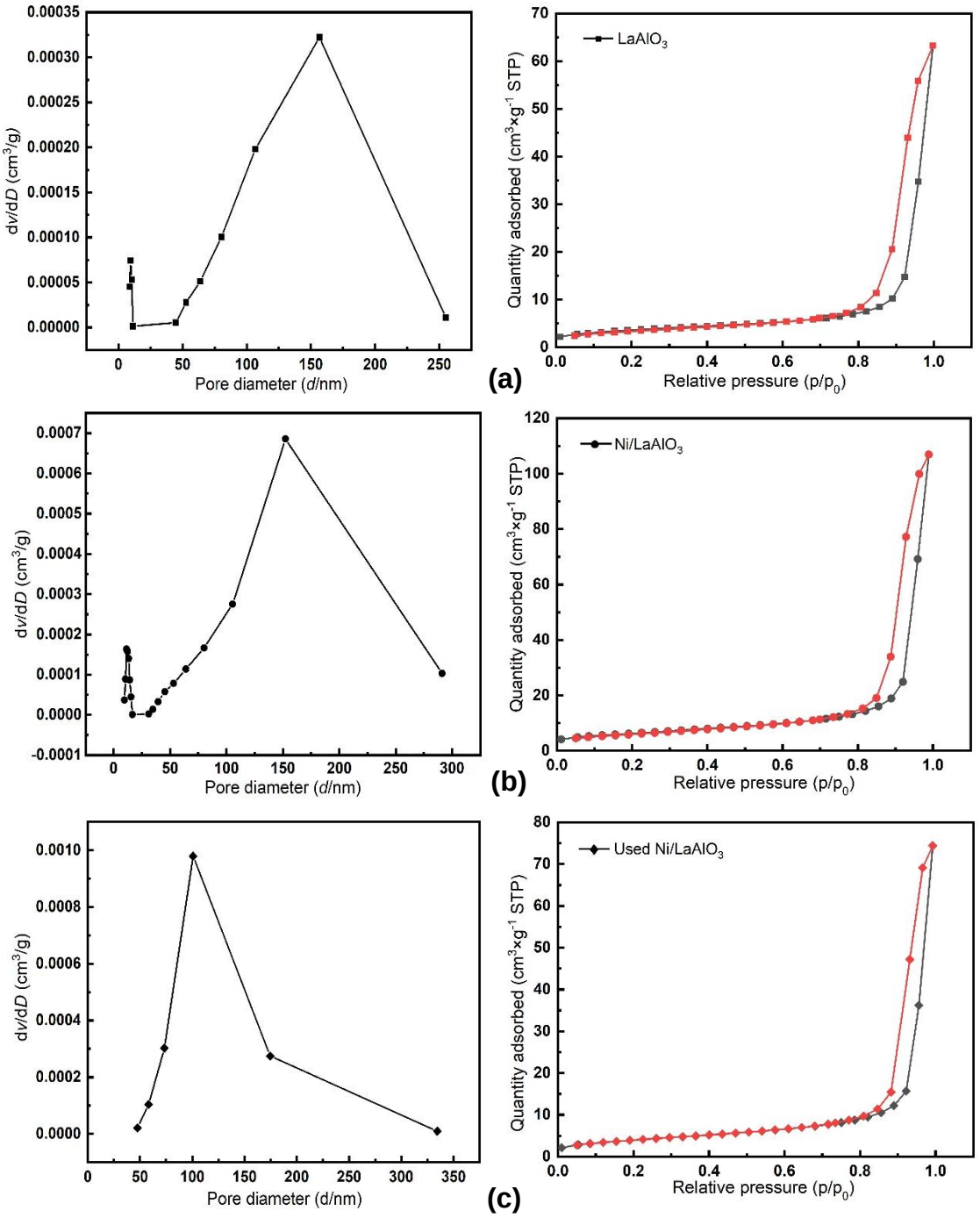

Fig. 6. The N_2 adsorption-desorption isotherm plots and BJH cumulative pore distribution of various catalysts: (a) $LaAlO_3$, (b) $Ni/LaAlO_3$, and (c) Used Ni/LaAlO

Application and Performance of Ni/$LaAlO_3$ Catalyst in Straw Fueled Pyrolysis

Effect of nickel load and reaction temperature on syngas production

Figure 7 shows the effect of the total amount of nickel load (from 5 wt% to 20 wt%) on syngas production at different reaction temperatures. During this test, the calcination temperature and holding time were fixed at 500 °C and 20 min, respectively. The yield of syngas produced *via* straw fueled pyrolysis was different as the total amount of nickel loaded was changed. When the nickel loading amount was 10 wt%, the H_2 and CO yield were the highest, and it was shown that when the reaction temperature increased, the H_2 and CO yield also gradually increased. These results were all based on the experiment with a 10 wt% nickel loaded catalyst.

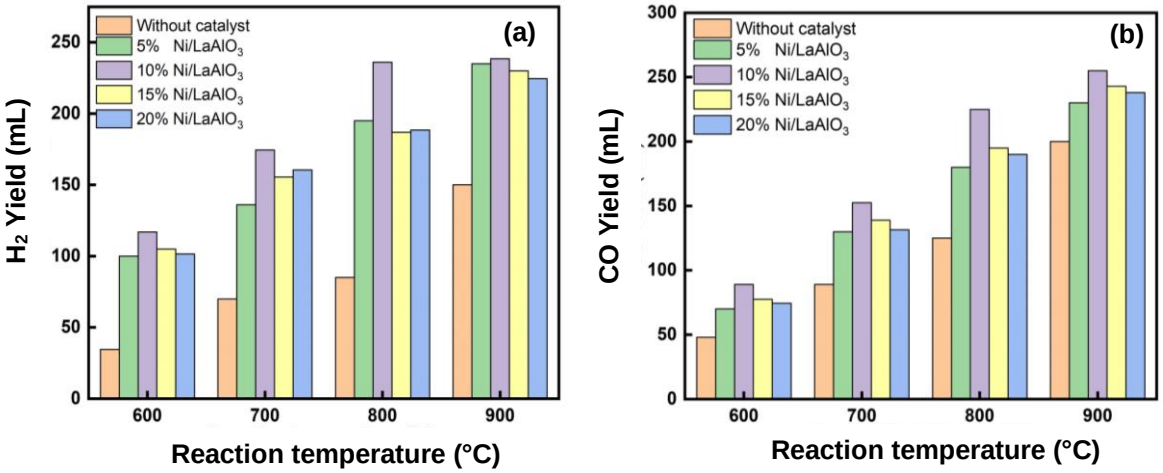

Fig. 7. Effect of Ni load and reaction temperature on the yield of syngas (a) H_2 and (b) CO

Effect of the reaction temperature

The effect of the reaction temperature (ranging from 600 °C to 900 °C) on the syngas concentration was studied with a total Ni loading amount of 10 wt%, a calcination temperature of 500 °C, and a holding time of 20 min. The dependence of the H_2 and CO concentration on the reaction temperature is depicted in Fig. 8, which conveyed that the gas concentration increased as the reaction temperature was increased when the SS was pyrolyzed without a catalyst. As the temperature was increased along the range of 600 °C to 900 °C, the H_2 and CO concentration experienced an upward trend, increasing from 16.86 vol% to 33.87 vol% and 18.05 vol% to 35.57 vol%, respectively. When the catalyst was added, the synthesis gas concentration drastically changed. As shown in Fig. 8, at the same reaction temperature, the concentration of H_2 and CO after the pyrolysis of SS with a Ni/$LaAlO_3$ catalyst was always higher than the concentration without catalyst. After using the catalyst, the H_2 and CO concentrations increased from 35.33 vol% and 26.98 vol% to 43.5 vol% and 42.67 vol%, respectively. However, as shown in Fig. 8, when the pyrolysis temperature rose from 800 °C to 900 °C, the H_2 and CO content increased from 43.1 vol% and 41.9 vol% to 43.5 vol% and 42.67 vol%, respectively. At 800 °C, the concentration of H_2 and CO increased from 23.5 vol% and 29.4 vol% to 43.1 vol% and 41.9 vol%, respectively, which was relatively low when compared to the increase in H_2 and CO content without a Ni/$LaAlO_3$ catalyst. As shown in Fig. 7, the production of H_2 and CO increased from 85 mL/g and 125 mL/g to 238.5 mL/g and 255 mL/g, respectively, so the optimal pyrolysis temperature was 800 °C.

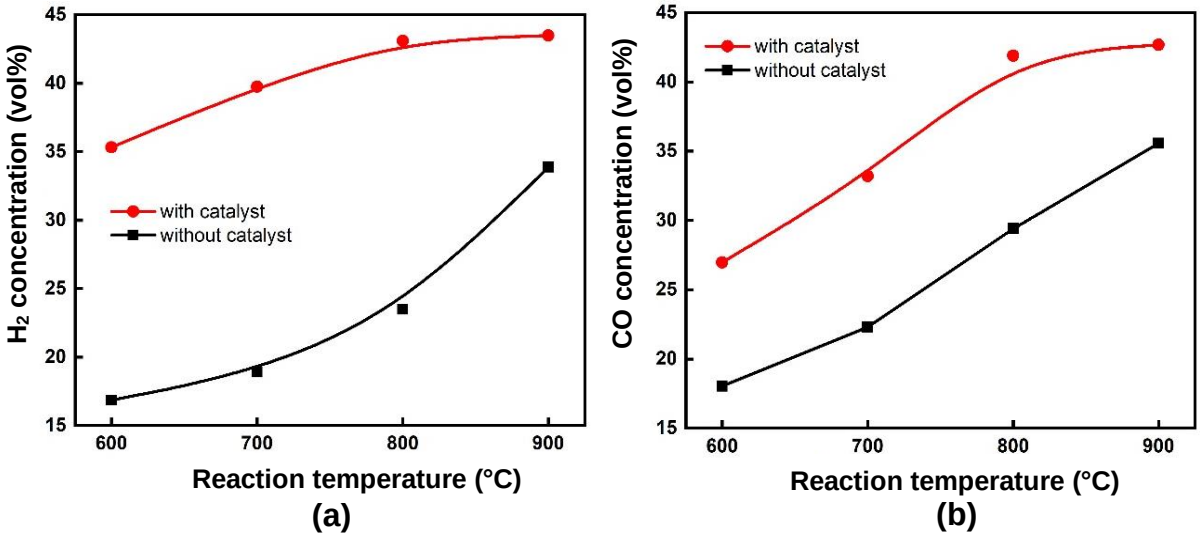

Fig. 8. Effect of the pyrolysis temperature on the syngas concentration: (a) H_2 and (b) CO

Effect of the holding time

The effect of the holding time (ranging from 5 min to 30 min) on the syngas concentration was studied with a total Ni loading amount of 10 wt%, a reaction temperature of 800 °C, and a calcination temperature of 500 °C. The dependence of the H_2 and CO concentration on the holding time is depicted in Fig. 9. As the holding time increased, the H_2 and CO concentrations also increased, but when the holding time exceeded 20 min, the concentration continued to only slightly increase; therefore, a holding time of 20 min was chosen. Compared with no catalyst at the same time, the addition of the $Ni/LaAlO_3$ catalyst, the H_2 and CO concentrations increased from 23.5 vol% and 29.4 vol% to 43.1 vol% and 41.9 vol%, respectively.

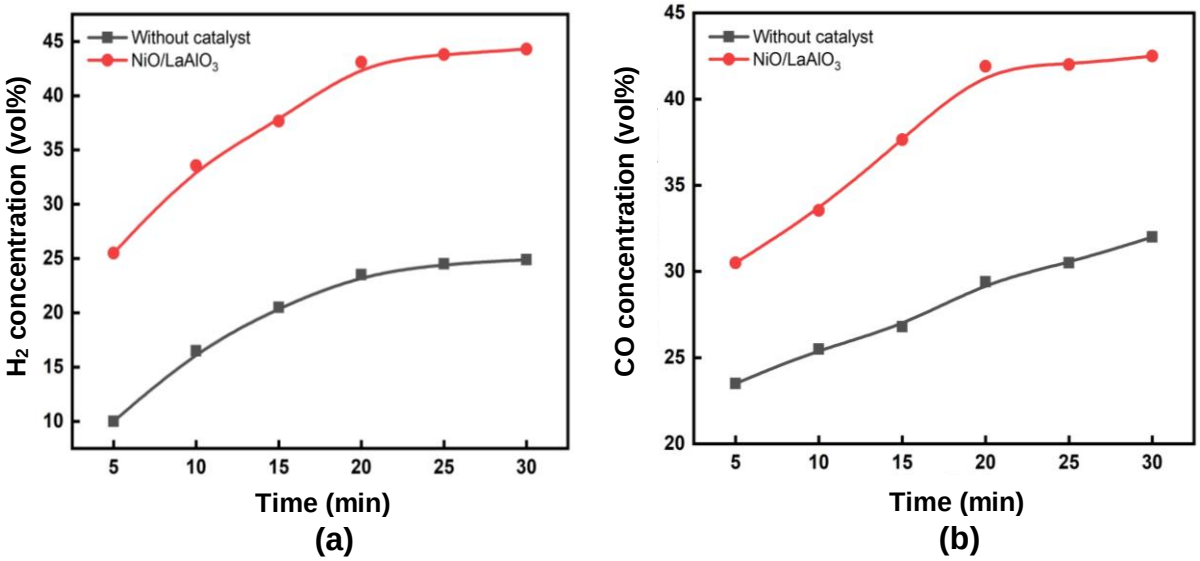

Fig. 9. Effect of the holding time on the syngas concentration: (a) H_2 and (b) CO

Effect of the calcination temperature

The effects of calcination temperature (ranging from 500 °C and 800 °C) on the syngas concentration was studied with a nickel loading, reaction temperature, and holding time of 10 wt%, 800 °C, and 20 min, respectively. Figure 10 shows the change in syngas concentration as the calcination temperature of the catalyst was increased. At a calcination temperature of 500 °C, the concentration of H_2 and CO reached its peak value of 43.1 vol% and 41.9 vol%, and the syngas concentration was 85 vol%. As the calcination temperature increased from 500 °C to 800 °C, the syngas concentration decreased from 85 vol% to 78 vol%, which indicated that the high calcination temperature decreased the catalyst activity.

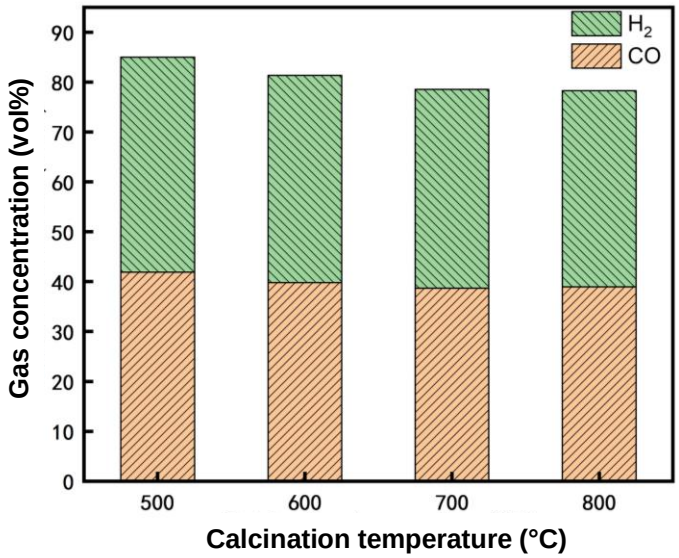

Fig. 10. Effect of the calcination temperature on the syngas concentration

Effect of the reuse times

The reuse times were obtained by cooling the catalyst to room temperature after doing one set of experiments and then conducting the next set of experiments. The effect of repeated usage of a $Ni/LaAlO_3$ catalyst on the catalytic effect was studied. As shown in Fig. 11, as the number of uses increased, the concentration of H_2 and CO decreased.

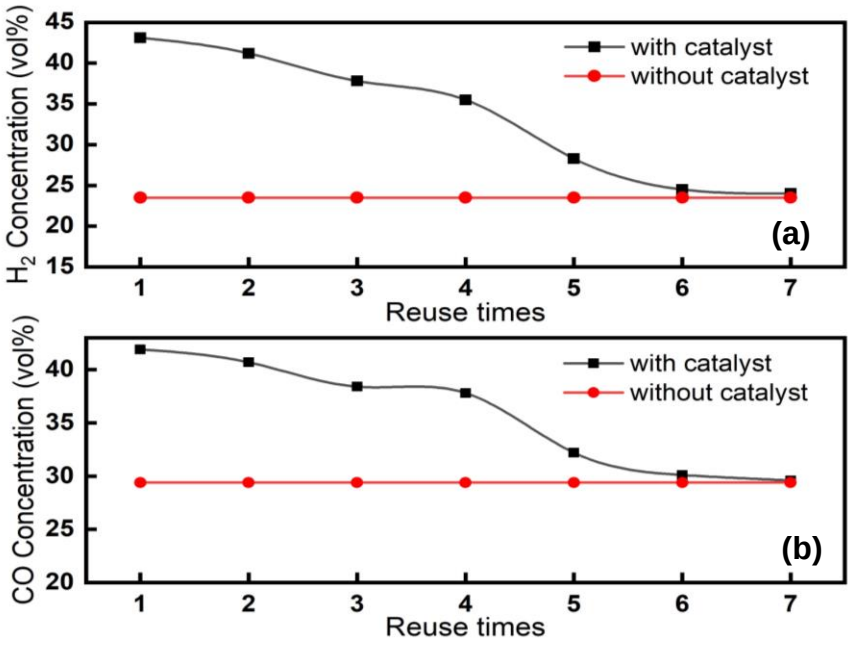

Fig. 11. Effect of the reuse times on the syngas concentration: (a) H_2 and (b) CO

Although the concentration of H_2 and CO decreased slightly in the first four experiments, they all exceeded 35 vol%. When used a fifth time, the concentration of H_2 and CO sharply decreased. During the sixth and seventh experiment, the concentration of H_2 and CO was nearly the same as that the concentrations recorded without a catalyst. This was attributed to the fact that more carbon deposits covered the active sites on the surface of the catalyst as the number of the use times increased, which led to lower catalytic activity of the catalyst (Qian and Kumar 2017).

CONCLUSIONS

1. The carrier prepared *via* the sol-gel method has good thermal stability. The nickel was uniformly loaded on the $LaAlO_3$ carrier *via* homogeneous precipitation, and the NiO uniformly dispersed on the surface of the carrier.
2. As the catalyst calcination temperature was increased from 500 °C to 800 °C, the synthesis gas concentration showed a downward trend.
3. The best performance with the usage of a $Ni/LaAlO_3$ catalyst for syngas preparation was obtained under the following conditions: a Ni loading amount of 10 wt%, a calcination temperature of 500 °C, a reaction temperature of 800 °C, and a holding time of 20 min.
4. When the reaction temperature was increased from 800 °C to 900 °C, although the synthesis gas concentration increased, the increase was not very obvious. The concentration of H_2 and CO increased from 43.1 vol% and 41.9 vol% at 800 °C to 43.5 vol% and 42.67 vol% at 900 °C, respectively.
5. A $Ni/LaAlO_3$ catalyst has good stability and can be reused 4 to 5 times

ACKNOWLEDGMENTS

The authors are grateful for the support of the building project of Hubei Province for the technology innovation and entrepreneurship service capacity Grant No. 2018BEC466 and for the Central Committee Guides Local Science and Technology Development Special Project of Hubei Province, Grant No. 2018ZYYD062.

REFERENCES CITED

Chein, R.-Y., and Fung, W.-Y. (2019). "Syngas production via dry reforming of methane over CeO_2 modified Ni/Al_2O_3 catalysts," *International Journal of Hydrogen Energy* 44 (28), 14303-14315. DOI: 10.1016/j.ijhydene.2019.01.113

Claude, V., Mahy, J. G., Geens, J., and Lambert, S. D. (2019). "Ni-doped γ-Al2O3 as secondary catalyst for bio-syngas purification: Influence of Ni loading, catalyst preparation, and gas composition on catalytic activity," *Materials Today Chemistry* 13, 98-109. DOI: 10.1016/j.mtchem.2019.05.002

Figueredo, G. P., Medeiros, R. L. B. A., Macedo, H. P., de Oliveira, Â. A. S., Braga, R. M., Mercury, J. M. R., Melo, M. A. F., and Melo, D. M. A. (2018). "A comparative study of dry reforming of methane over nickel catalysts supported on perovskite-type $LaAlO_3$ and commercial α-Al_2O_3," *International Journal of Hydrogen Energy* 43(21), 11022-11037. DOI: 10.1016/j.ijhydene.2018.04.224

Gao, N., Han, Y., Quan, C., and Wu, C. (2017). "Promoting hydrogen-rich syngas production from catalytic reforming of biomass pyrolysis oil on nanosized nickel-ceramic catalysts," *Applied Thermal Engineering* 125, 297-305. DOI: 10.1016/j.applthermaleng.2017.07.028

GB/T 28731-2012 (2012). "Proximate analysis of solid biofuels," Standardization Administration of China, Beijing, China.

Hossain, M. A., Jewaratnam, J., and Ganesan, P. (2016). "Prospect of hydrogen production from oil palm biomass by thermochemical process – A review," *International Journal of Hydrogen Energy* 41(38), 16637-16655. DOI: 10.1016/j.ijhydene.2016.07.104

Hu, M., Laghari, M., Cui, B., Xiao, B., Zhang, B., and Guo, D. (2018). "Catalytic cracking of biomass tar over char supported nickel catalyst," *Energy* 145, 228-237. DOI: 10.1016/j.energy.2017.12.096

Li, C., Hirabayashi, D., and Suzuki, K. (2009). "Development of new nickel based catalyst for biomass tar steam reforming producing H_2-rich syngas," *Fuel Processing Technology* 90(6), 790-796. DOI: 10.1016/j.fuproc.2009.02.007

Li, D., Koike, M., Chen, J., Nakagawa, Y., and Tomishige, K. (2014). "Preparation of Ni–Cu/Mg/Al catalysts from hydrotalcite-like compounds for hydrogen production by steam reforming of biomass tar," *International Journal of Hydrogen Energy* 39(21), 10959-10970. DOI: 10.1016/j.ijhydene.2014.05.062

Li, Q., Ji, S., Hu, J., and Jiang, S. (2013). "Catalytic steam reforming of rice straw biomass to hydrogen-rich syngas over Ni-based catalysts," *Chinese Journal of Catalysis* 34(7), 1462-1468. DOI: 10.1016/S1872-2067(12)60618-4

Li, W., Li, F., Wang, H., Liao, M., Li, P., Zheng, J., Tu, C., and Li, R. (2020). Hierarchical mesoporous ZSM-5 supported nickel catalyst for the catalytic hydrodeoxygenation of anisole to cyclohexane," *Molecular Catalysis* 480, 1-8. DOI: 10.1016/j.mcat.2019.110642

Lian, G. A. O., Jing, L. I. U., Qing, Z., and Peng, Z. (2018). "Research progress of Ni-based composite catalysts for methane dry reforming," *Journal of Inorganic Materials* 33, 1-11. DOI: 10.15541/jim20170585

Lim, S., Moon, D., Kim, J., Kim, Y., Park, N., and Shin, J. (2007). "Autothermal reforming of propane over Ni catalysts supported on a variety of perovskites," *Journal of Nanoscience and Nanotechnology* 7(11), 4013-4016. DOI: 10.1166/jnn.2007.093

Lim, S.-S., Lee, H.-J., Moon, D.-J., Kim, J.-H., Park, N.-C., Shin, J.-S., and Kim, Y.-C. (2009). "Autothermal reforming of propane over Ce modified Ni/LaAlO3 perovskite-type catalysts," *Chemical Engineering Journal* 152(1), 220-226. DOI: 10.1016/j.cej.2009.03.054

Loy, A. C. M., Yusup, S., Lam, M. K., Chin, B. L. F., Shahbaz, M., Yamamoto, A., and Acda, M. N. (2018). "The effect of industrial waste coal bottom ash as catalyst in catalytic pyrolysis of rice husk for syngas production," *Energy Conversion and Management* 165, 541-554. DOI: 10.1016/j.enconman.2018.03.063

Qian, K., and Kumar, A. (2017). "Catalytic reforming of toluene and naphthalene (model tar) by char supported nickel catalyst," *Fuel* 187, 128-136. DOI: 10.1016/j.fuel.2016.09.043

Saxena, R. C., Adhikari, D. K., and Goyal, H. B. (2009). "Biomass-based energy fuel through biochemical routes: A review," *Renewable and Sustainable Energy Reviews* 13(1), 167-178. DOI: 10.1016/j.rser.2007.07.011

Tan, R. S., Abdullah, T. A. T., Mahmud, S. A., Zin, R. M., and Isa, K. M. (2019). "Catalytic steam reforming of complex gasified biomass tar model toward hydrogen over dolomite promoted nickel catalysts," *International Journal of Hydrogen Energy* 44(39), 21303-21314. DOI:10.1016/j.ijhydene.2019.06.125

Wei, Q., Gao, X., Liu, G., Yang, R., Zhang, H., Yang, G., Yoneyama, Y., and Tsubaki, N. (2018). "Facile one-step synthesis of mesoporous Ni-Mg-Al catalyst for syngas production using coupled methane reforming process," *Fuel* 211, 1-10. DOI: 10.1016/j.fuel.2017.08.093

Xiao, X., Cao, J., Meng, X., Le, D. D., Li, L., Ogawa, Y., Sato, K., and Takarada, T. (2013). "Synthesis gas production from catalytic gasification of waste biomass using nickel-loaded brown coal char," *Fuel* 103, 135-140. DOI: 10.1016/j.fuel.2011.06.077

Xu, L., Song, H., and Chou, L. (2013). "Ordered mesoporous $MgO–Al_2O_3$ composite oxides supported Ni based catalysts for CO_2 reforming of CH_4: Effects of basic modifier and mesopore structure," *International Journal of Hydrogen Energy* 38(18), 7307-7325. DOI: 10.1016/j.ijhydene.2013.04.034

Zhao, Z., and Yan, H. (2012). "Assessment of the biomass power generation industry in China," *Renewable Energy* 37(1), 53-60. DOI: 10.1016/j.renene.2011.05.017

Zou, X., Chen, T., Liu, H., Zhang, P., Ma, Z., Xie, J., and Chen, D. (2017). "An insight into the effect of calcination conditions on catalytic cracking of toluene over 3Fe8Ni/palygorskite: Catalysts characterization and performance," *Fuel* 190, 47-57. DOI: 10.1016/j.fuel.2016.11.038

Zhao, G., Chai, R., Zhang, Z., Sun, W., Liu, Y., and Lu, Y. (2019). "High-performance Ni-$CeAlO_3$-Al_2O_3/FeCrAl-fiber catalyst for catalytic oxy-methane reforming to syngas," *Fuel* 258. DOI: 10.1016/j.fuel.2019.116102

Article submitted: February 27, 2020; Peer review completed: April 18, 2020; Revised version received and accepted: June 9, 2020; Published: June 15, 2020.
DOI: 10.15376/biores.15.3.5871-5885
ERRATUM: August 27, 2020: Units in the text were changed on pages 5880-5881 from wt% to vol%. These edits do not change the conclusions of the paper.